Fermilab FERMILAB-FN-0694 February 2001

The Fermilab Proton Driver Painting Injection Simulations*

A. Drozhdin, O. Krivosheev
Fermi National Accelerator Laboratory
P.O. Box 500, Batavia, Illinois 60510

January 3, 2001

Abstract

Summary of studies is presented towards beam injection design optimization in the 16 GeV Fermilab Proton Driver. Painting injection system, which consists of two sets of fast horizontal and vertical magnets, permits to realize uniform density distribution of the circulating beam at injection required for the beam space charge effect reduction. Analytical formulas for stripping efficiency, proton hits distribution and average number of hits upon the stripping foil are written and the results of analytical calculations are verified with numerical simulations. The temperature buildup during injection pulse and steady state temperature of the foil are calculated from analytical distributions of the proton hits.

1 Introduction

A 16 GeV Proton Driver lattice parameters [1] are presented in Table 1.

There are three $48m$ long straight sections in the ring. One of them, called below "utility section", is used for the beam injection, extraction and collimation [2], and two others are used for RF cavities. The Proton Driver beta functions and dispersion along the accelerator and in the utility section are shown in Figures 1 and 3.

The beam extraction system is located at the first half part of the utility section. It consists of $3.5m$ length vertical kicker magnet and three Lam-

*Work supported by the U. S. Department of Energy under contract No. DE-AC02-76CH03000

Kinetic energy at injection	0.4 GeV
Extraction kinetic energy	16 GeV
Circumference	647.9 m
Injected beam normalized transverse emittance (95%)	$3 \cdot mm.mrad$
Normalized transverse emittance after painting	$60 \cdot mm.mrad$
Painting injection duration	90 μs (27 turns)
Protons per bunch at injection	$8.25 \cdot 10^{12}$
Protons per bunch at extraction	$7.5 \cdot 10^{12}$
Number of bunches	4
Total intensity at injection	$3.3 \cdot 10^{13}$
Total intensity at extraction	$3 \cdot 10^{13}$
Repetition rate	15 Hz
Longitudinal emittance	2 $eV \cdot s$
RF frequency at injection	1.20 MHz
RF frequency at extraction	1.69 MHz
RF voltage	1.2 MV
$SIN(\varphi_s)$ at injection	0.087266
Horizontal betatron tune	10.78991
Vertical betatron tune	10.50717
Horizontal beta at the foil	20.083 m
Horizontal α at the foil	-0.686
Horizontal dispersion at the foil	0.68 m
Vertical beta at the foil	11.870 m
Vertical α at the foil	0.587
Horizontal beam size at injection in the foil	$\sigma_x = 3.1\ mm$
Vertical beam size at injection in the foil	$\sigma_y = 2.4\ mm$

Table 1: Proton Driver parameters.

bertson magnets (Lamb-1, 2, 3) which extract the beam from accelerator in horizontal plane (Figure 3).

The beam halo collimation system [3] is used to localize proton losses in a specially shielded short section of accelerator, and so to reduce irradiation of the rest part of the ring to acceptable level. It consists of two primary, and seven secondary collimators located in a drift spaces of the last two accelerator lattice cells upstream of and in the first half part of the utility section.

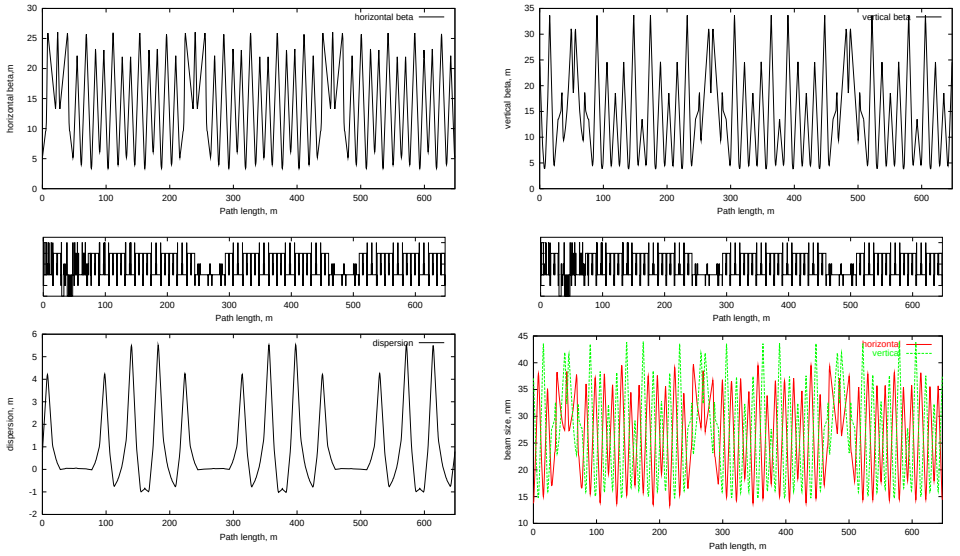

Figure 1: 16 GeV Proton Driver beta functions, dispersion and beam size after painting.

2 Painting Injection

Painting injection is required to realize uniform density distributions of the beam in the transverse plane. It is performed by using two sets of horizontal and vertical fast magnets (kickers). Proton orbit is moved in the horizontal plane at the beginning of injection by 46.3 mm to the thin graphite stripping foil to accept first portion of protons generated by the H^- in the foil (Figure 2). Three 0.5 m long kicker magnets are used to produce orbit displacement (Figure 3). Maximum field of magnets is 0.35 kG. Horizontal kick for beam painting is shown in Figure 4. Gradual reduction of the kickers strength permits to "paint" the injected beam across the accelerator aperture with required emittance. Vertical kicker magnets located in the injection line (not shown here) provide injected beam angle sweeping during injection time, starting from maximum at the beginning of injection and going to zero at the end of painting process. Horizontal and vertical kickers cause particles betatron amplitude variation during injection, that results to uniform distribution of the circulating beam after painting. Painting starts from the central region of phase space in horizontal plane and from the border of it in the vertical plane, and goes to the border of the beam in horizontal plane and to the center in the vertical plane. This produces elliptical cross section

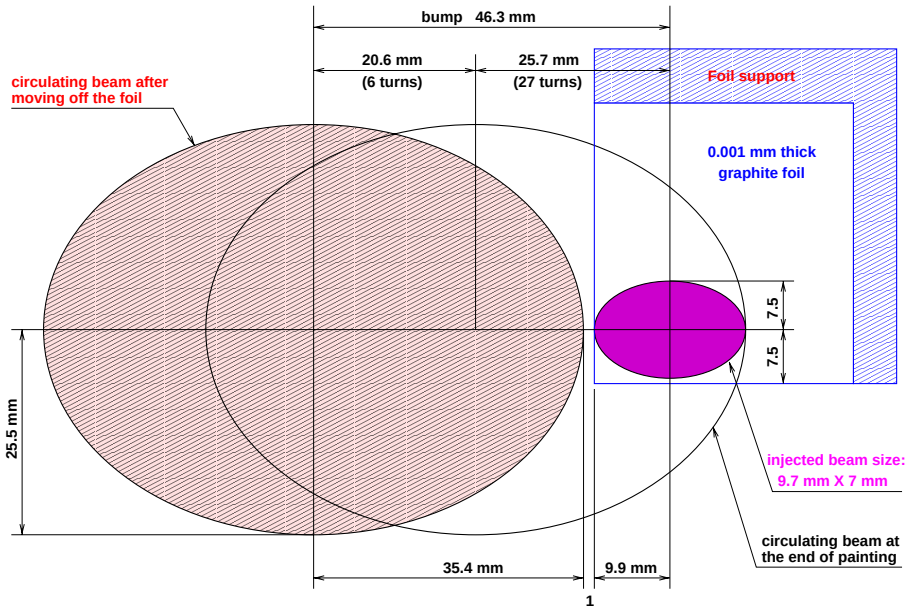

Figure 2: Injected and circulating beams location in the foil at painting.

of the beam eliminating particles with maximum amplitudes in both planes simultaneously.

Beam painting reduces beam space charge effect and results to the beam emittance preservation at injection. The beam size in the utility section after painting is presented in Figure 4.

Two $1.5m$ long accelerator magnets located from both sides of the foil (bump-magnets in Figure 3) are used to separate the proton and H^- beams at the quadrupole triplet upstream of the foil by 638 mm and at the collimator downstream of the foil. This allows for the H^- beam to pass outside of the quadrupole body. Beam dump located behind the stripping foil is used for H^o components interception. Three more magnets (two - upstream, and one - downstream of the separation magnets) are used for dispersion compensation outside of the injection region (Figure 5). Horizontal dispersion in the foil is equal to $0.68m$. This scheme does not need usually used special large aperture bump magnets and septum-magnet to transport H^- beam outside the accelerator quadrupole, but unfortunately it brakes periodicity of accelerator.

A multi-turn particle tracking through the accelerator is done with the

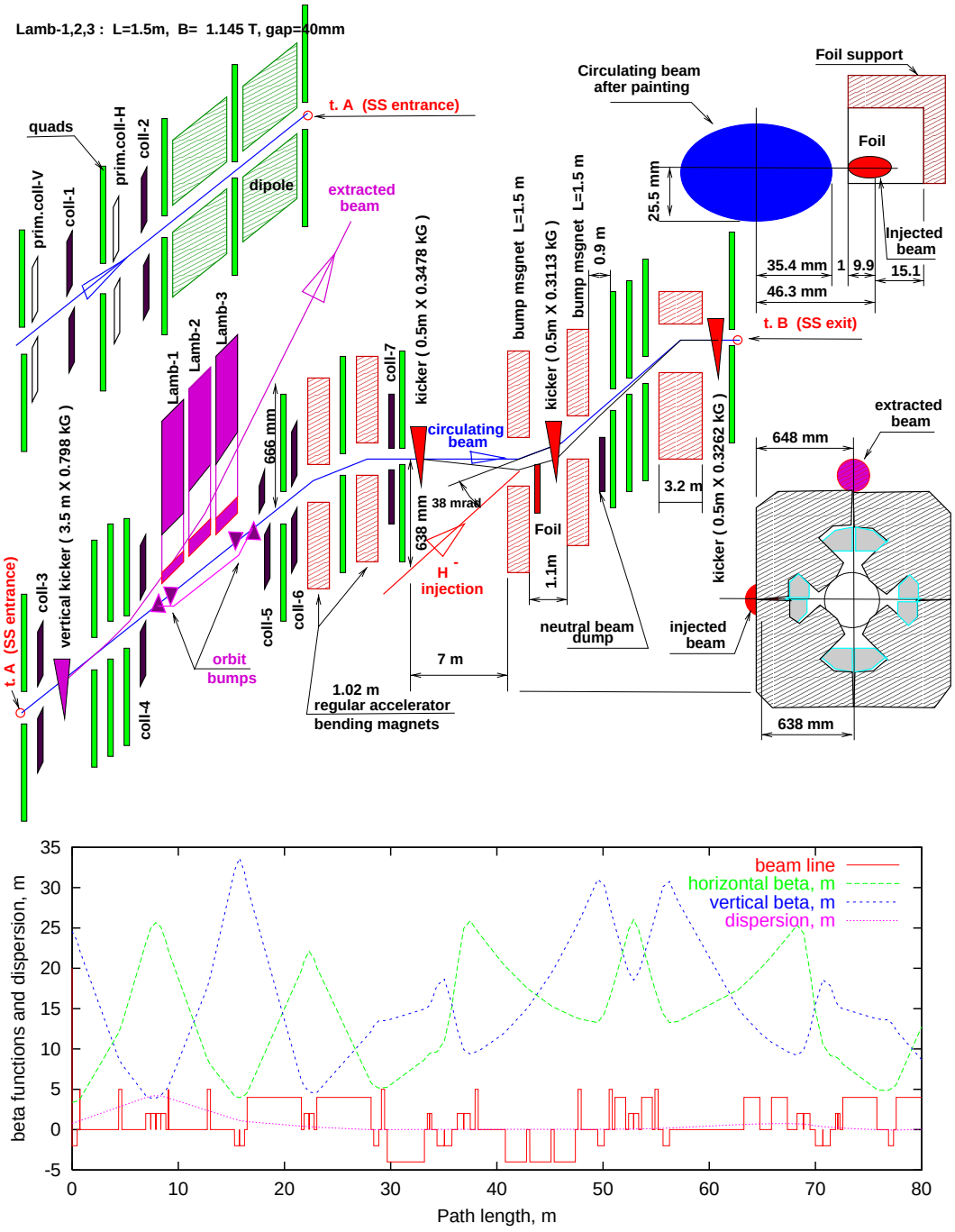

Figure 3: Beam extraction, collimation and beam painting schemes location and beta functions and dispersion in the utility section.

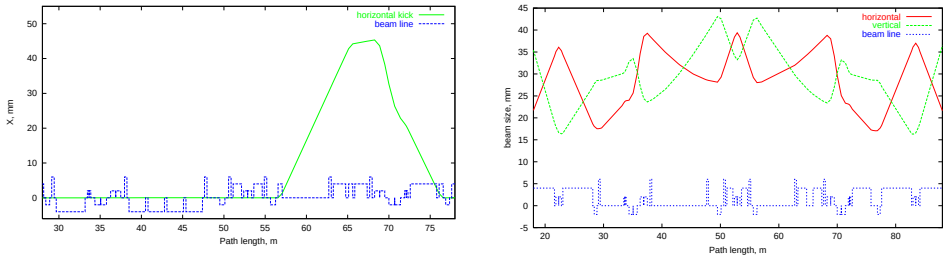

Figure 4: Horizontal kick for beam painting (left) and beam size after painting (right).

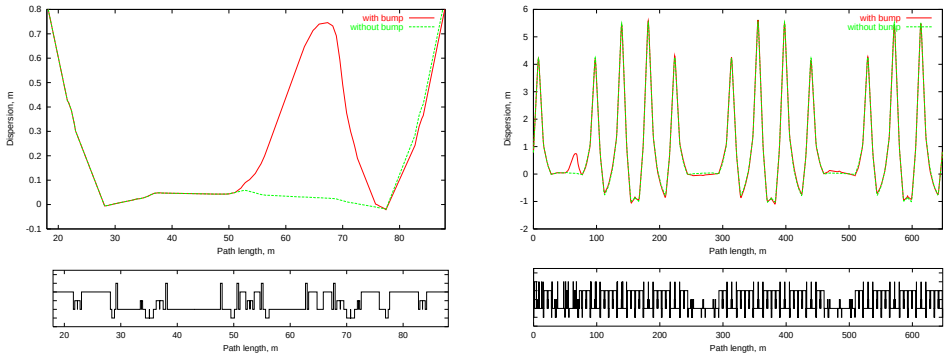

Figure 5: Horizontal dispersion with beam separation for injection.

STRUCT [4] code. A stripping foil made of $300\mu g/cm^2$ (1.5 μm) thick graphite is located between the separation magnets. The foil has the shape of so-called corner foil, where two edges of the square foil are supported and the other two edges are free. The foil size is $2.5cm \times 2.5cm$.

The dependence of kicker-magnets strength on time is chosen to get uniform distribution of the beam after painting both in horizontal and vertical planes. An optimal waveform of bump-magnets [5] was simulated in the STRUCT code as presented below:

- in horizontal plane

$$B = B_o \left[0.445 + 0.555 \left(1 - \sqrt{\frac{2\ N}{27} - \left(\frac{N}{27}\right)^2} \right) \right] \qquad N < 27 \qquad (1)$$

$$B = B_o \left[0.445 - \frac{N - 27}{13.483} \right] \qquad N > 27 \qquad (2)$$

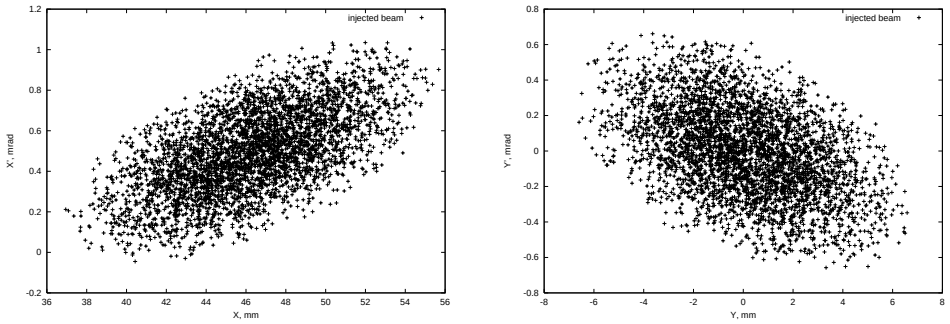

Figure 6: Horizontal (left) and vertical (right) phase plane in the foil at injection.

- in vertical plane

$$Y' = Y'_o\sqrt{2\frac{27-N}{27} - \left(\frac{27-N}{27}\right)^2} \qquad Y'_o = 1.509\ mrad \qquad (3)$$

Here N - turn number from the beginning of painting.

Horizontal phase plane of injected beam in the foil is shown in Figure 6. Emittance of injected beam at 95% is equal to $3mm \cdot mrad$.

Painting lasts during 27 turns, and after painting the circulating beam moves out of the foil during 6 turns to complete particles interaction with the foil. In the simulations horizontal bump amplitude at the foil is 46.3 mm = 25.7 mm (painting) + 20.6 mm (removing from the foil) (Figure 2), vertical angle variation is $1.509\,mrad$. Horizontal and vertical phase plane of circulating beam in the foil at 6-th, 28-st, and 33-d turns from the beginning of beam painting are presented in Figure 7.

Horizontal bump-magnet strength and vertical angle of the beam in the foil during injection are presented in the top of Figure 8. Particle transverse population and particle density distribution in the foil after painting are shown in the middle and at the bottom of Figure 8. The beam painting bump functions are chosen to get uniform distribution of the beam for betatron tunes which are far from low order betatron resonances. Unfortunately vertical betatron tune is close to half integral, that causes nonuniform vertical distribution of the beam after painting. This can be fixed by tuning the accelerator off the resonance.

Average number of hits upon the stripping foil for each particle is as low as 3.72. This effects low level nuclear interactions and multiple Coulomb

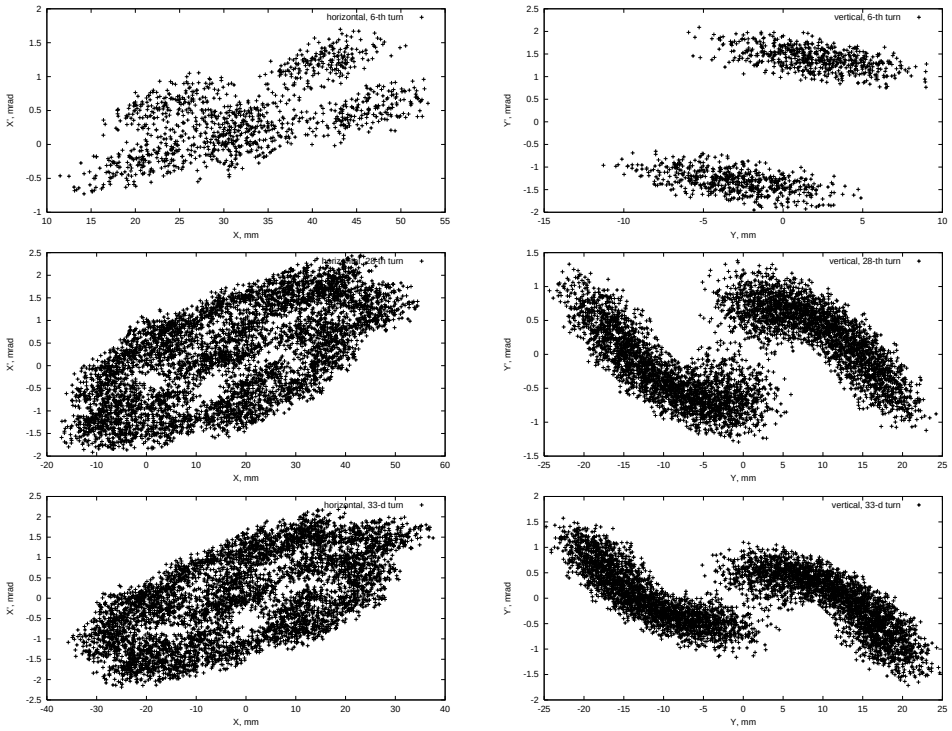

Figure 7: Horizontal (left) and vertical (right) phase plane in the foil at 6-th (top), 28-th (middle), and 33-d (bottom) turn from the beginning of beam painting.

scattering in the foil at injection, and because of this causes low level particle loss at injection.

Circulating beam protons pass several times through the foil and some of them can be lost because of scattering in the foil. A multiple Coulomb scattering angle is very small because of small thickness of the foil. Particle energy loss in the foil at one pass is $0.7 \cdot 10^{-6}$. The rate of nuclear interactions in the foil during the total process is $3.7 \cdot 10^{-5}$. The emittance of circulating beam in horizontal plane is small in the beginning of painting and it gradually reaches the maximum only at the end of painting. Therefore horizontal amplitude of particles, in average, is sufficiently less compared to the accelerator aperture. Particles can be lost only during the first few turns after injection, and only in the region of injection kick maximum where the beam is close to accelerator aperture. At every next turn after particles were injected, they move out of the aperture restriction because of fast reduction

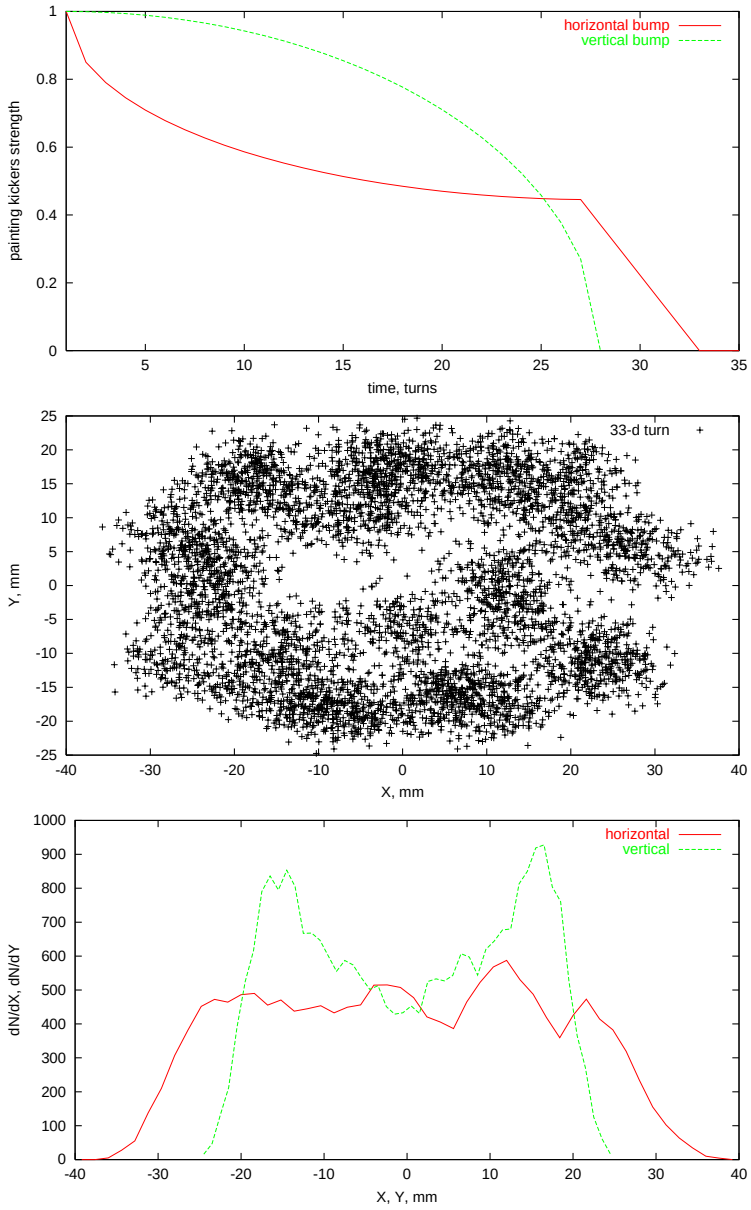

Figure 8: Horizontal bump-magnet strength and vertical angle of the beam at injection in the foil (top). Particle transverse population (middle) and particle density distribution in the foil (bottom) at 33-d turn from the beginning of beam painting.

of painting kick amplitude. Simulations shown that the rate of particle loss in the accelerator at interaction with foil is as low as $7.4 \cdot 10^{-5}$.

3 Analytical calculations of proton distribution and temperature raise upon the stripping foil

The standard notation was used in the next section, namely c is the speed of light, $\hbar$ is the Planck constant, k is the Boltzmann constant, $m_e c^2$ is the electron rest mass, r_e is classical electron radius, N_a is the Avogadro number, σ_{SB} is the Stefan-Boltzmann constant, M and E are particles mass and kinetic energy, $\beta = \frac{|\vec{v}|}{c}$ is particle speed N_i is the number of particles injected per turn, σ_x and σ_y are r.m.s. for Gaussian distribution of injected beam at the foil, A,Z and I are mass, charge and ionization potential of foil atoms, ρ, c_p, κ and ε are the material density, specific heat, thermal conductivity and emissivity.

3.1 Deposited energy density

The energy deposited by protons into the foil by the beam can come from nuclear or electromagnetic interactions. We do not consider contribution from nuclear interaction due to very small foil thickness usually used in the painting setup. With nuclear interaction length in the tens of centimeters the interaction probability is less then 10^{-6}.

The density of deposited energy from proton source in $\frac{GeV}{cm^3 \cdot sec}$ during one injection pulse is:

$$S(\vec{r}, t) = \frac{N}{2\pi\sigma^2} \cdot |\frac{dE}{dz}| \cdot e^{-r^2/2\sigma^2} \cdot \delta(t) \tag{4}$$

where $\delta(t)$ is Dirac's delta-function. It is properly normalized, so that the total energy deposition is

$$S_{total} = \int_V d^3\vec{r} \int dt\, S(\vec{r}, t) = N \cdot |\frac{dE}{dz}| \cdot \Delta z$$

where Δz is the foil thickness. From Review of Particle Physics [8] the ionization energy loss - the main energy deposition source in the case of thin foil - can be written as Bethe-Bloch expression:

$$-\frac{dE}{dz} = K \cdot \frac{Z}{A} \cdot \frac{1}{\beta^2}[\frac{1}{2} \log \frac{2m_e c^2 \beta^2 \gamma^2 T_{max}}{I^2} - \beta^2 - \frac{1}{2}\delta] \tag{5}$$

where K is equal to $4\pi N_a r_e^2 m_e c^2$ ($0.307075\ \frac{MeV \cdot cm^2}{g}$), T_{max} is the maximum energy transfer in one collision and can be written:

$$T_{max} = \frac{2m_e c^2 \beta^2 \gamma^2}{1 + 2\gamma m_e/M + (m_e/M)^2}.$$

and δ is density correction, calculated according to Sternheimer approximation.

3.2 Heat propagation

The heat propagation in 3D can be described by Fourier-Kirchoff equation:

$$c_p \rho \frac{\partial T}{\partial t} = \vec{\nabla}(\kappa(\vec{r}) \cdot \vec{\nabla} T) + S(\vec{r}, t) \tag{6}$$

We don't take into account cooling due to emission yet. If κ doesn't depend on coordinates, the equation (6) could be rewritten as

$$\frac{\partial T}{\partial t} = a(\vec{\nabla}^2 T) + \frac{S(\vec{r}, t)}{\rho \cdot c_p}, \tag{7}$$

where a is equal to $\kappa/c_p\rho$ ($cm^2 \cdot sec^{-1}$). In order to solve (7) we put the heat transfer equation with $\delta(\vec{r}, t)$ source and look for Green's function. If we're looking for Green's function of the heat transfer equation without sources, heat transfer equation can be easily written as follows

$$\frac{\partial T}{\partial t} - a(\vec{\nabla}^2 T) = \delta(\vec{r}, t). \tag{8}$$

Green's function for above equation is well-known [9] and can be written as follow for 3D case:

$$G_{3d}(\vec{r_0} - \vec{r}, t_0 - t) = \frac{\theta(t_0 - t)}{(2\sqrt{a\pi(t_0 - t)})^3} e^{-\frac{(\vec{r_0} - \vec{r})^2}{4a(t_0 - t)}}, \tag{9}$$

and for 2D case (no heat propagation in z direction):

$$G_{2d}(\vec{r_0} - \vec{r}, t_0 - t) = \frac{\theta(t_0 - t)}{4\pi a(t_0 - t)} e^{-\frac{(\vec{r_0} - \vec{r})^2}{4a(t_0 - t)}}. \tag{10}$$

It is now quite easy to get the heat distribution using convolution of Green's function and heat source:

$$T(\vec{r_0}, t_0) = T_0 + \frac{1}{\rho c_p} \int_V d^3\vec{r} \int dt\, G(\vec{r_0} - \vec{r}, t_0 - t) \cdot S(\vec{r}, t).$$

For 2D case we can get following expression using source term (4) and 2D Green's function (10):

$$T(\vec{r},t) = T_0 + \frac{N}{2\pi\sigma^2\rho c_p} \cdot |\frac{dE}{dz}| \cdot \frac{\theta(t)}{1+2at/\sigma^2} e^{-\frac{\vec{r}^2}{2\sigma^2(1+2at/\sigma^2)}}. \qquad (11)$$

If we do have injection pulses following each other after τ seconds, then source term (4) will be transformed into

$$S(\vec{r},t) = \frac{N}{2\pi\sigma^2} \cdot e^{-r^2/2\sigma^2} \cdot \sum_{j=0}^{n} \delta(t-j\tau), \qquad (12)$$

where n is equal to $[t/\tau]$. Therefore, the solution (11) will be rewritten into

$$T(\vec{r},t) = T_0 + \frac{N}{2\pi\sigma^2\rho c_p} |\frac{dE}{dz}| \sum_{j=0}^{n} \frac{\theta(t-j\tau)}{1+2a(t-j\tau)/\sigma^2} e^{-\frac{\vec{r}^2}{2\sigma^2(1+2a(t-j\tau)/\sigma^2)}}. \quad (13)$$

Considering the maximum temperature point $\vec{r}=0$, it is easy to get analytical expression for $T(\vec{0},t)$:

$$T(\vec{0},t) = T_0 + \frac{N}{4\pi a\tau\rho c_p} |\frac{dE}{dz}| \, [\psi(-\frac{\sigma^2+2at}{2a\tau}) - \psi(n+1-\frac{\sigma^2+2at}{2a\tau})],$$

where $\psi(x)$ is digamma (logarithm derivative of $\Gamma(x)$) function [11].

3.3 Heat emission

The another mechanism to dissipate heat after the pulse of injection is a heat emission. It is quite obvious that it is predominant way of the heat dissipation due to very small foil thickness.

The energy emission of the black body is proportional to the temperature in the forth power, the Stefan-Boltzmann law:

$$Q = \sigma_{SB} \cdot T^4.$$

Stefan-Boltzmann law is applicable for any material if we define the material emissivity ε as the ratio between particular material heat emission and equivalently heated black body. Therefore, the heat propagation equation with emission as the only mechanism to cool the foil is

$$\frac{\partial T}{\partial t} = \frac{S(\vec{r},t)}{\rho c_p} - \frac{2\varepsilon\sigma_{SB}}{\Delta z \rho c_p} \cdot (T^4 - T_0^4), \qquad (14)$$

We will solve (14) in two steps. First, consider time interval from 0 to very small ϵ. Emission did not change the temperature, therefore the only viable will be source term and after integration over t from 0 to ϵ we have

$$T_\epsilon = T_0 + \frac{1}{\rho c_p}\frac{N}{2\pi\sigma^2}|\frac{dE}{dz}|e^{-r^2/2\sigma^2}. \tag{15}$$

Then we'll solve the equation

$$\frac{\partial T}{\partial t} = -\frac{\varepsilon\sigma_{SB}}{\Delta z\rho c_p}\cdot(T^4 - T_0^4), \tag{16}$$

starting from time point ϵ and using T_ϵ (15) as initial value. Integration of (16) gives us the implicit equation for $T(t)$ dependence:

$$-\frac{\varepsilon\sigma_{SB}}{\Delta z\rho c_p}(t-\epsilon) = \frac{1}{2T_0^3}[\arctan\frac{T_\epsilon}{T_0} - \arctan\frac{T}{T_0}] + \frac{1}{4T_0^3}[\log\frac{T-T_0}{T_\epsilon - T_0} - \log\frac{T+T_0}{T_\epsilon + T_0}]. \tag{17}$$

In order to get the solution of (14) it is obvious we have to get the limit $\epsilon \to 0$. Such limit only removes ϵ from the right part of equation (16). For clearness, we provide the explicit dependence in the next equation

$$t = \frac{\Delta z\rho c_p}{4T_0^3\varepsilon\sigma_{SB}}[\arctan\frac{T_0(T(\vec{r},t) - T_\epsilon(\vec{r}))}{T_0^2 + T_\epsilon(\vec{r})T(\vec{r},t)} + \frac{1}{2}\log\frac{(T_\epsilon(\vec{r}) - T_0)\cdot(T(\vec{r},t) + T_0)}{(T_\epsilon(\vec{r}) + T_0)\cdot(T(\vec{r},t) - T_0)}]. \tag{18}$$

But it is probably impossible to get explicit dependence $T(\vec{r},t)$ trying to reverse (17), therefore numerical solution is required.

The solution might be greatly simplified if we consider the case when T_0 is equal to 0. In that case the equation (16) will be rewritten into

$$\frac{\partial T}{\partial t} = -\frac{2\varepsilon\sigma_{SB}}{\Delta z\rho c_p}\cdot T^4 \tag{19}$$

with initial temperature being $T_\epsilon = \frac{N}{2\pi\sigma^2\rho c_p}|\frac{dE}{dz}|\exp(-\vec{r}^2/2\sigma^2)$. The solution is quite simple

$$\frac{1}{T^3} - \frac{1}{T_\epsilon^3} = \frac{3\varepsilon\sigma_{SB}}{\Delta z\rho c_p}(t-\epsilon),$$

which after taking the limit $\epsilon \to 0$ and resolving relative to T gives us the final answer:

$$T = T_\epsilon \cdot \sqrt[3]{\frac{\Delta z\rho c_p}{6\varepsilon\sigma_{SB}T_\epsilon^3 t + \Delta z\rho c_p}}.$$

To find the temperature behavior at injection than pulses follow each other with τ seconds between them (see (12)), it is easy to write down the recursive procedures for the temperature at the given time

$$\begin{aligned} T_{j\tau} &= T_{\epsilon+(j-1)\tau} \cdot^3 \sqrt{\frac{\Delta z \rho c_p}{3\varepsilon\sigma_{SB} T^3_{\epsilon+(j-1)\tau} \cdot \tau + \Delta z \rho c_p}}, \\ T_{j\tau+\epsilon} &= T_{j\tau} + \frac{N}{2\pi\sigma^2 \rho c_p} |\frac{dE}{dz}| \exp(-\bar{r}^2/2\sigma^2), \\ T(j\tau < t < (j+1)\tau) &= T_{j\tau+\epsilon} \cdot^3 \sqrt{\frac{\Delta z \rho c_p}{3\varepsilon\sigma_{SB} T^3_{j\tau+\epsilon} \cdot t + \Delta z \rho c_p}}. \end{aligned}$$

Same scheme can be written for $T(t)$ dependence when T_0 is not equal to 0, but from (18) it is obvious that $T_{j\tau}$ and $T(j\tau < t < (j+1)\tau)$ could be obtained only numerically.

3.4 Beam painting and foil heating

We have to take into account the beam movement and therefore the source change during painting. The following notation is used below: x^k_n and y^k_n being the center of injected bunch. Index k is the turn index while n denotes the injection index. There are some conditions on k and n, namely $0 \le n \le N_c = 27$ and $n \le k \le N_c + N_f$, where N_f is the number of turns for beam removal from the foil at the end of injection. The circulating orbit position (1, 2):

$$\begin{aligned} x^o_k &= x_0\{p_0 + p_1 \cdot [1 - \sqrt{\frac{2k}{N_c} - (\frac{k}{N_c})^2]}\} \qquad N \le 27 \\ x^o_k &= x_0 \cdot p_0\{1 - \frac{k - N_c}{N_f}\} \qquad N > 27 \\ y^o_k &= 0 \end{aligned}$$

where p_0 and p_1 denotes orbit position at the end of painting and amplitude of the closed orbit bump during the painting process. Obviously, $p_0 + p_1 \equiv 1$. As was mentioned early, painting starts from the center of the beam in horizontal plane and from large amplitude in a vertical plane, producing an elliptical cross section of the circulating beam. The beam is injected to the ellipse with current transverse amplitudes (3) of

$$x^e_n = p_1 \cdot x_0 \cdot \sqrt{\frac{2n}{N_c} - (\frac{n}{N_c})^2}$$

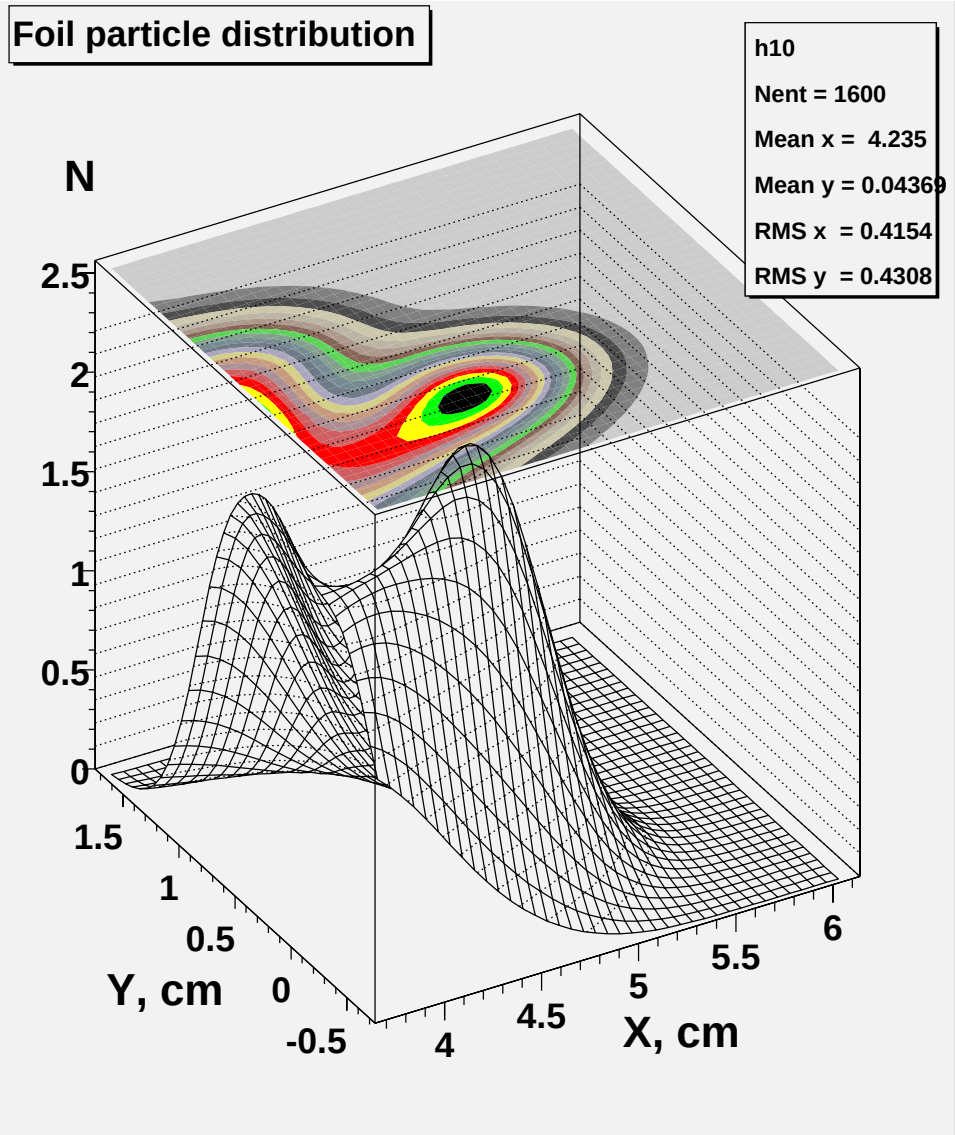

Figure 9: Proton hits distribution upon the stripping foil at painting injection.

$$y_n^e = y_0\sqrt{2\cdot\frac{N_c-n}{N_c}-(\frac{N_c-n}{N_c})^2}$$

We now can write down the expression for x_n^k and y_n^k. Knowing the

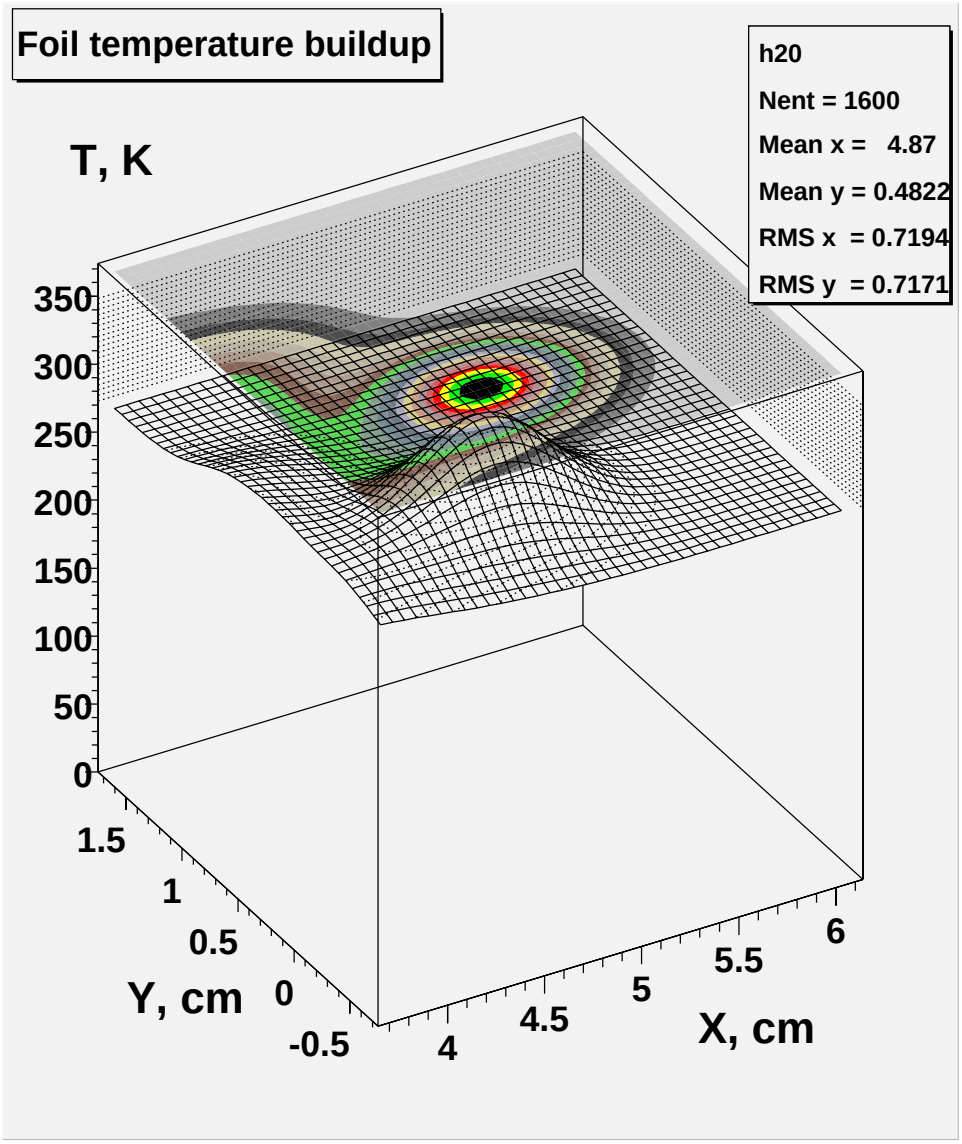

Figure 10: Stripping foil temperature buildup after one cycle of particles injection to the proton driver.

horizontal and vertical tunes ν_x and ν_y

$$\begin{aligned} x_n^k &= x_k^o + x_n^e \cdot \cos[2\pi\nu_x(k-n)] \\ y_n^k &= y_k^o + y_n^e \cdot \cos[2\pi\nu_y(k-n) - \pi/2] \end{aligned}$$

or if we define N_i as number of particles injected in one cycle, the proton density $S_N(\vec{r},t)$ will be

$$S_N(\vec{r},t) = \frac{N_i}{2\pi\sigma_x\sigma_y}\sum_{n=0}^{N_c}\sum_{k=n}^{N_c+N_f} e^{-(x-x_n^k)^2/2\sigma_x^2-(y-y_n^k)^2/2\sigma_y^2}$$

and for foil with left lower corner (x_{ll}, y_{ll}) and upper right corner (x_{ur}, y_{ur}) we can get the average number of collisions as the result of integration

$$< N_{col} >= \frac{1}{N_c \cdot N_i}\int_{x_{ll}}^{x_{ur}} dx \int_{y_{ll}}^{y_{ur}} dy\, S_N(\vec{r},t)$$

Integrating this one can get

$$\begin{aligned} < N_{col} > &= \sum_{n=0}^{N_c}\sum_{k=n}^{N_c+N_f} [erf(\frac{x_{ur}-x_n^k}{\sqrt{2}\sigma_x}) + erf(\frac{x_n^k - x_{ll}}{\sqrt{2}\sigma_x})] \cdot \\ & [erf(\frac{y_{ur}-y_n^k}{\sqrt{2}\sigma_y}) + erf(\frac{y_n^k - y_{ll}}{\sqrt{2}\sigma_y})]/4N_c \end{aligned}$$

Next, very similar expression gives us the total energy deposited in the foil:

$$\begin{aligned} E_{tot} &= \frac{\Delta z}{4N_c}\sum_{n=0}^{N_c}\sum_{k=n}^{N_c}[|\frac{dE_p}{dz}| + 2|\frac{dE_e}{dz}|\delta_{n,k}][erf(\frac{x_{ur}-x_n^k}{\sqrt{2}\sigma_x}) + \\ & erf(\frac{x_n^k - x_{ll}}{\sqrt{2}\sigma_x})][erf(\frac{y_{ur}-y_n^k}{\sqrt{2}\sigma_y}) + erf(\frac{y_n^k - y_{ll}}{\sqrt{2}\sigma_y})] \end{aligned}$$

3.5 Solution for heat transfer and heat emission

If we have both heat emission and heat transfer the equation become more complicated. Combining (7) and (14) together, one can get

$$\frac{\partial T}{\partial t} = a(\vec{\nabla}^2 T) + \frac{S(\vec{r},t)}{\rho c_p} - \frac{2\varepsilon\sigma_{SB}}{\Delta z \rho c_p}\cdot(T^4 - T_0^4), \tag{20}$$

The only way to solve such equation is numerically, using code such as ANSYS [10].

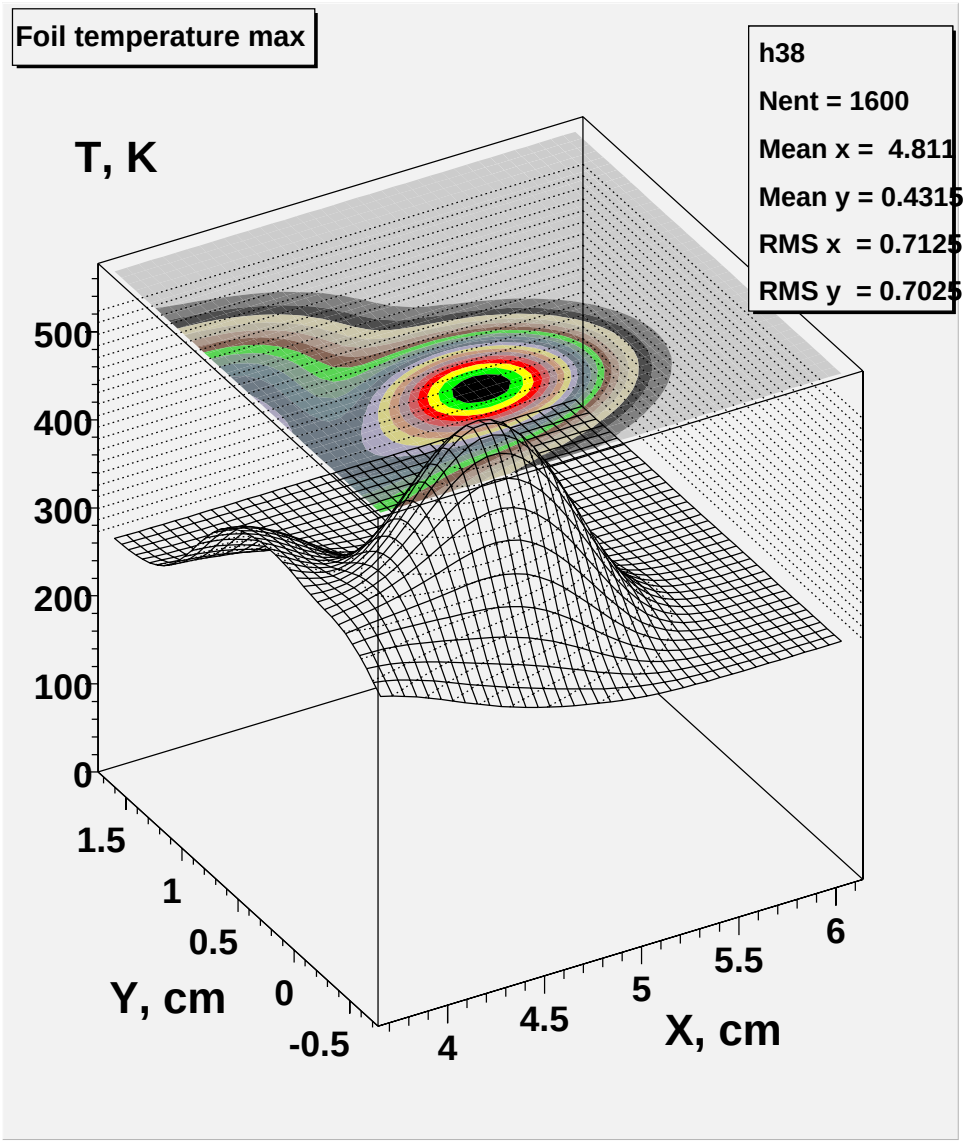

Figure 11: Steady state maximum temperature distribution in the stripping foil at painting injection to the proton driver.

3.6 Stripping efficiency

Most of injected H^- are stripped into protons in the foil and the rest into each excited state of $H^o(n)$ atoms, where n is the principal quantum number

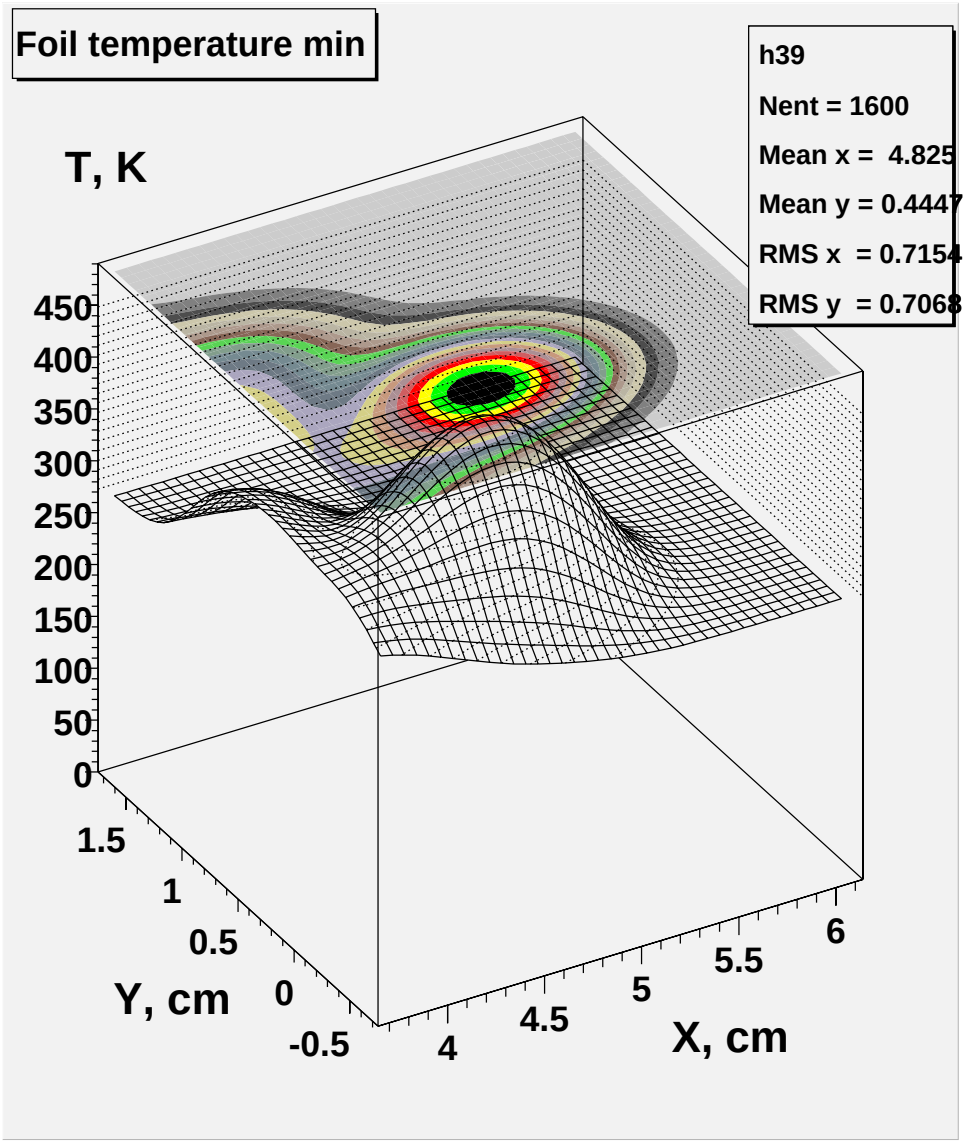

Figure 12: Steady state minimum temperature distribution in the stripping foil at painting injection to the proton driver.

of the excited state. Some excited states decay into protons on the way to H^o dump. Those particles become a beam halo, and are lost somewhere else in the ring or are intercepted by the collimation system. Defining σ_{if}

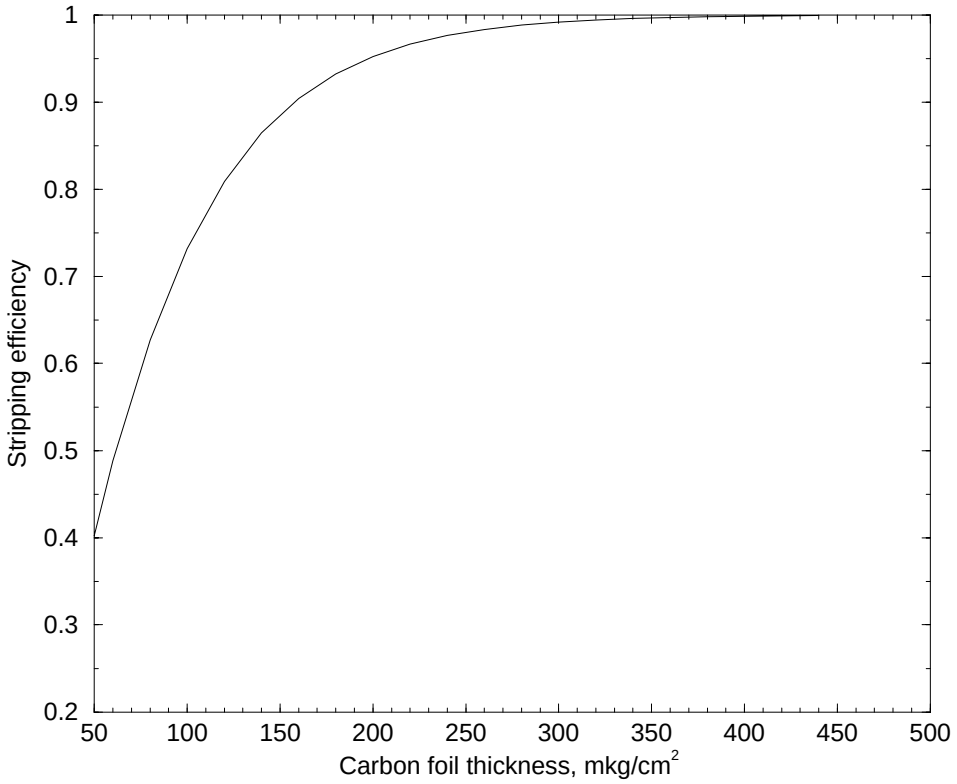

Figure 13: Carbon foil stripping efficiency.

as cross-section for the process $H^i \rightarrow H^f + (f-i)e^-$ we could write the stripping efficiency (Figure 13)

$$N_+ = 1 - \frac{\sigma_{-10}\exp\{-\sigma_{01}x\} - (\sigma_{01}-\sigma_{-11})\exp\{-(\sigma_{-10}+\sigma_{-11})x\}}{\sigma_{-10}+\sigma_{-11}-\sigma_{01}}$$

Number of $\mathrm{H}^o(n)$ atoms in a highly excited state ($n \geq n_{ex}$), assuming the yield of excited state, is proportional to n^{-3}:

$$Y(n \geq n_{ex}) = (1-N_+)\cdot\frac{\sum_{n=n_{ex}}^{\infty} n^{-3}}{\sum_{n=1}^{\infty} n^{-3}} = (1-N_+)\cdot\frac{\psi'(n_{ex})}{\psi'(1)}$$

4 Results of analytical calculations

In this part we try to estimate the foil stripping efficiency, the proton hits distribution and foil temperature after 400 MeV proton beam injection into

the machine during 27 turns with following beam removal from the foil during 6 turns.

The calculations are done in following assumptions:

1. Electrons are stripped immediately and then pass through the foil independently;
2. Nuclear interactions in the foil are negligible small, therefore the main energy deposition sources for a very thin foil are proton restricted ionization energy loss $-\frac{dE_p}{dz} \cdot \frac{\Delta z}{<\cos\theta_p>} \simeq -\frac{dE_p}{dz} \cdot \Delta z$ and electron energy loss during stripping phase $-2\frac{dE_e}{dz} \cdot \frac{\Delta z}{<\cos\theta_e>}$. Here Δz is a foil thickness and $< \cos\theta_p > \simeq 1$ and $< \cos\theta_e >$ are proton and electron angle at stripping.
3. At the kinetic energy of $\approx$ 218keV for electrons accompanied this process the range and $-\frac{dE_e}{dx}$ according to the ICRU37 are $580 \cdot 10^2 \frac{\mu g}{cm^2}$ and $2.4\frac{MeV \cdot cm^2}{g}$ respectively. Therefore we assume electron contribution to the heating is approximately equal to -2$\frac{dE_e}{dx}\Delta s_e$;

For the carbon foil parameters:

- density $\rho = 2.0\frac{g}{cm^3}$
- thickness $\Delta z = 300\frac{\mu g}{cm^2}$
- specific heat $c_p = 0.165\frac{cal}{g \cdot K}$
- thermal conductivity $\kappa = 0.057\frac{cal}{cm \cdot K \cdot sec}$
- emissivity $\varepsilon = 0.80$

the calculated stripping efficiency is 99.2% and estimated yield of excited states $H^o(n)$ atoms with $n \geq 5$ is equal to 0.016%. These atoms will be stripped into protons before they get the dump and become a beam halo. The rest excited states atoms ($n \leq 4$) have a longer lifetime and they will go to the neutral beam dump.

An average number of proton hits on the foil (3.72) found from simulations is very close to that was calculated analytically (3.80).

The proton hits distribution calculated from formulas above (Figure 9) was used for foil temperature buildup and steady state temperature calculations.

Due to pretty large size of H^- beam at the foil, small number of collisions and small electron contribution, the temperature buildup in the foil per pulse is less than 100K (Figure 10).

The heat emission cooling of the foil due to the Stefan-Boltzmann law

$$Q = \varepsilon \cdot \sigma_{SB} \cdot T^4$$

at this temperature is small. With only emission as a cooling mechanism the foil temperature reaches a steady state after about 10 pulses with maximum temperature of 540K (Figure 11) and minimum around 450K (Figure 12).

5 Conclusions

Painting injection system, which consists of two sets of fast horizontal and vertical magnets, permits to realize quasi-uniform density distribution of the circulating beam required for the beam space charge effect reduction and emittance preservation at injection.

The analytical formulas for stripping efficiency proton hits distribution and average number of hits upon the stripping foil are written and the results of analytical calculations are verified with numerical simulations.

The calculated stripping efficiency is 99.2%, and estimated yield of excited states $H^o(n)$ atoms with $n \geq 5$ is equal to 0.016%. These atoms become a beam halo.

The temperature buildup during injection pulse and steady state temperature of the foil are calculated from analytical distribution of proton hits. An instant temperature buildup, calculated with contributions of multiple collisions, ionization loss from protons and electrons accompanied stripping process, is a little bit less then 100K.

With only emission as a cooling mechanism the foil temperature reaches a steady state of $\sim$ 500K after 10 cycles of injection that is less then 1 second.

References

[1] D. Ritson, 16 *GeV* Proton Driver Lattice, Private communications, December 1999.

[2] A. Drozhdin, C Johnstone and N. Mokhov,'16 GeV Proton Driver Beam Collimation System', ICFA Mini-Workshop on High-Intensity, High-Brightness Hadron Beams "Beam Halo and Scraping", September 13-15, 1999 * Interlaken Resort on Lake Como, Wisconsin.

[3] A. Drozhdin, O. Krivosheev, N. Mokhov, "Beam Loss, Collimation and Shielding at the Fermilab Proton Driver", Fermilab–FN–693 (2000).

[4] I. Baishev, A. Drozhdin, and N. Mokhov, 'STRUCT Program User's Reference Manual', SSCL–MAN–0034 (1994), http://www-ap.fnal.gov/ drozhdin/STRUCT/STR2.html

[5] 'JHF Accelerator Design Study Report', KEK Report 97-16, JHF-97-10, March 1998, p3-67 - 3-71..

[6] O. Krivosheev and N. Mokhov,'Tolerable beam losses and shielding', ICFA Mini-Workshop on High-Intensity, High-Brightness Hadron Beams "Beam Halo and Scraping", September 13-15, 1999 * Interlaken Resort on Lake Como, Wisconsin.

[7] N. V. Mokhov, 'The MARS Code System User's Guide, Version 13(95)', Fermilab–FN–628 (1995).

[8] Review of Particle Physics, Particle Data Group, The European Physical Journal, v. 15, 2000.

[9] V. .S. Vladimirsky, *Mathematical Physics Equations,* Moscow, "Nauka", 1981.

[10] "ANSYS User's Manual", Vol. I and II, SASI Publications, 1994.

[11] M. Abramowitz and I. A. Stegun, "Handbook of Mathematical Functions", Dover Publications, Inc., New York, 1970.